ChemSusChem

Research Article
doi.org/10.1002/cssc.202400661

Chemistry Europe
European Chemical Societies Publishing

www.chemsuschem.org

Gas-Phase Photocatalytic Coprocessing of CO_2 – $H_2O_{(v)}$ to Energy Products Promoted by the *n,n*-Junction In_2O_3@g-C_3N_4 under VIS-Light

Tomasz Baran,[a] Michele Aresta,*[a] Roberto Comparelli,[b] and Angela Dibenedetto*[c]

Carbon dioxide capture and utilization is a strategic technology for moving away from fossil-C. The conversion of CO_2 into fuels demands energy and hydrogen that cannot be sourced from fossil-C. Co-processing of CO_2 and water under solar irradiation will have a key role in the long-term for carbon-recycling and energy products production. This article discusses the synthesis, characterization and application of the two-phase composite photocatalyst, In_2O_3@g-C_3N_4, formed by thermal condensation of melamine in the presence of indium(III)nitrate. The composite exhibits a *n,n*-heterojunction between two *n*-type semiconductors, g-C_3N_4 and In_2O_3, leading to a more efficient charge separation. The composite has a flat band potential enabling it to effectively catalyze the reduction of CO_2 in the gas phase to produce CO, CH_4 and CH_3OH. While the composite's overall photocatalytic efficiency is comparable to that of neat g-C_3N_4, its ability to promote multielectron-transfer and Proton Coupled to Electron Transfer (PCET) suggests that there is a potential for further optimization of its properties. The use of labelled $^{13}CO_2$ has allowed us to clearly exclude that the reduced species are derived from the photocatalyst decomposition or the degradation of contaminants.

Introduction

In recent years, graphitic carbon nitride (g-C_3N_4) has emerged as a highly promising, sustainable and versatile material in photocatalysis, drawing attention due to its unique structural characteristics.[1–3] The building block of g-C_3N_4 is tri-s-triazine, a hexagonal ring composed of three nitrogen and three carbon atoms (Figure 1).[4,5] The tri-s-triazine units are linked together through nitrogen atoms to form a planar, graphitic-like structure. As a two-dimensional polymer composed of carbon and nitrogen with extended electron delocalization, g-C_3N_4 exhibits a suitable bandgap for the efficient absorption of visible light (band gap energy between 2.8 and 3 eV).[6] As a matter of fact, such material is an excellent promoter of solar-driven photocatalytic reactions. The chemical stability and metal-free composition further contribute to its appealing application in the development of new processes powered by sustainable energy such as solar energy. So far, graphitic carbon nitride has been applied in photocatalytic applications such as degradation of organic pollutants,[1,2,6–8] generation of hydrogen[9–12] or inactivation of microorganisms.[13,14] A particularly interesting application of g-C_3N_4 is in the photochemical-PC or photoelectrochemical-PEC reduction of carbon dioxide (CO_2).[15,16]

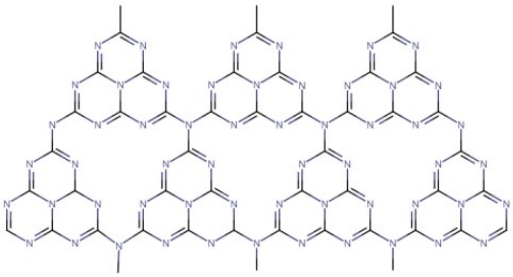

Figure 1. Structure of graphitic carbon nitride g-C_3N_4.

The global commitment to mitigate climate change expressed at the recent COP28 (December 2023) *via* transitioning away from fossil fuels, has intensified research efforts towards the utilization of solar energy and finding alternative carbon sources. CO_2, together with biomass and plastic waste recycling, is a potential source of carbon, the most abundant and easy to reach. Therefore, developing viable strategies and novel materials for CO_2 conversion into value-added products is gaining momentum all over the world.[17,18] Among them photocatalysis and photoelectrocatalysis appear as most promising strategies.[19–21] In this context, the use of g-C_3N_4 to harness

[a] *T. Baran, M. Aresta*
Innovative Catalysis for Carbon Recycling-IC²R, Tecnopolis, Lab 019–020, via Casamassima km 3, 70010 Valenzano-BA, Italy
E-mail: michele.aresta@ic2r.com

[b] *R. Comparelli*
CNR-IPCF, Istituto per i Processi Chimico-Fisici, S.S. Bari, c/o Dipartimento di Chimica, Via Orabona 4, 70126 Bari, Italy

[c] *A. Dibenedetto*
CIRCC, via Celso Ulpiani 27, 70126 Bari, Italy
and
Department of Chemistry, University of Bari Aldo Moro, Campus Universitario, Bari, 70125, Italy
E-mail: angela.dibenedetto@uniba.com

Supporting information for this article is available on the WWW under https://doi.org/10.1002/cssc.202400661

solar energy and catalyze the transformation of carbon dioxide into C_1-hydrocarbons (CH_4) or other C_1-compounds (CO, CH_2O, CH_3OH) or even C_n species, offers a hopeful road for addressing both energy and environmental challenges.

Recently we have found that bulk doping of graphitic carbon nitride[6,22] and modification by metal oxides[3,12] improve the photocatalytic efficiency of g-C_3N_4. In particular, the presence of CuO as a co-catalyst on g-C_3N_4 causes the H_2 production-rate to increase by a factor of 10 compared to the pristine material. Similarly, a higher photoactivity was observed when g-C_3N_4 was doped with iron, cobalt, zinc, manganese, antimony or bismuth, mainly due to an enlarged light absorption range. Moreover, the addition of a co-catalyst seems to be a leitmotif for enhancing the activity of the composite In_2O_3@g-C_3N_4 heterojunction that is usually used in the presence of sacrificial organic donors. So, In_2O_3/g-C_3N_4 decorated with 3 wt% Pt exhibits hydrogen production *via* water reduction in the presence of 10 vol% TEOA as a sacrificial agent.[23] Several papers have reported the use of In_2O_3@g-C_3N_4 composites in the degradation of organics in water or water added with H_2O_2.[24–26] In_2O_3@g-C_3N_4 has also found application in water disinfection under irradiation.[27] A very recent paper has reported that In_2O_3@g-C_3N_4 loaded with $Co(bpy)_3^{2+}$ as co-catalyst reduces CO_2 to CO in the presence of triethanolamine.[28] We have also reported that the formation of composites of indium oxide with other semiconductors results in improved opto-electronic properties.[29] In this paper, we present the synthesis, characterization and application of graphitic carbon nitride modified with indium oxide as the first example of In_2O_3@g-C_3N_4 (without any additional co-catalyst) able to reduce CO_2 to CO, CH_3OH, and CH_4 with water oxidation, without any sacrificial organic electron-donors.

Experimental

Synthesis of Materials

Synthesis of g-C_3N_4

Pure g-C_3N_4 was prepared by thermal treatment. 1.0 g of melamine (Sigma–Aldrich) was grounded in an agate mortar to obtain a fine homogeneous powder, which was then placed in a porcelain crucible. The latter was heated in a muffle furnace to reach 600 °C and annealed for 3 hours. After cooling to room temperature, the resulting solid mass was ground into a powder using a mortar.

Synthesis of In_2O_3@g-C_3N_4

1.0 g of melamine (Sigma-Aldrich) was grounded in an agate mortar along with indium nitrate (0.053, 0.106 or 0.265 g) (Alfa Aesar) until a uniform mixture was achieved. The amount of indium nitrate was such that the end-material contained 2%, 10% or 25% w/w of In-metal, shown through the paper as X%In_2O_3@g-C_3N_4, where X refers to the % of In-metal and not In_2O_3. The mixture of melamine and metal salt was placed in a porcelain crucible, heated in a muffle furnace to reach 600 °C and annealed for 3 hours. After cooling to room temperature, the resulting solid mass formed by In_2O_3@g-C_3N_4 was grounded into a powder using a mortar.

Synthesis of In_2O_3

In_2O_3 was obtained by calcination of indium nitrate (100 mg, supplier: Alfa Aesar) at 550 °C in air for 2 h.

Characterization of the Materials

UV-Vis Diffuse Reflectance Spectra (DRS) were recorded using a UV-2700i spectrophotometer (Shimadzu) equipped with an integrating sphere (ISR-2600Plus). Powder samples were grounded with $BaSO_4$ (Alfa Aesar) in a 1:80 w/w ratio. Barium sulphate was used as a reference. FTIR analysis was performed using IR-Spirit spectrophotometer (Shimadzu) with an ATR attachment. XRD analysis was performed using Panalytical Empyrean with PIXel3D detector. Scanning electron microscopy (SEM) studies were conducted using a Quanta FEG 250 microscope under low vacuum conditions at a pressure of 70 Pa with a beam accelerating voltage of 5 kV. Energy-dispersive X-ray spectroscopy (EDS) analyses were carried out under low vacuum conditions at a pressure of 20 Pa with a beam accelerating voltage of 10 kV or 30 kV using the EDAX Octane SDD detector.

Electrochemical Characterization

Photoelectrochemical measurements were carried out using the BioLogic SP-150 potentiostat. The working electrode was made by depositing the photocatalyst on FTO-glass (fluorine-doped tin oxide); a silver chloride electrode and a platinum spiral were used as the reference and the counter electrode, respectively. The scan rate was 10 mV/s. An XBO lamp was used as the light source. The illumination was from the front side. The electrolyte was purged with N_2 before each measurement. A 0.1 M phosphate buffer (adjusted with KOH to pH = 7) was used as an electrolyte. Electrochemical impedance measurements were recorded at a constant frequency while sweeping the electrode potential; Mott-Schottky tests were performed with the potential ranging from −0.6 V to +1.2 V, using two different frequencies of 1 and 2.5 kHz. Open Circuit Potential (OCP) determination is described in the SI.

Tests on the Photocatalytic Activity

5.0 mg of photocatalyst were sonicated with 100 μL of distilled water for 20 min. The suspension was uniformly distributed on the internal wall of a glass vial (total volume 10 mL, closed with a screw cap equipped with a teflon/silicon septum) and the vial (without the cap) dried at 90 °C for 1 h under vacuum using a vacuum-N_2 line, avoiding the contact with oxygen. The vial was then filled with carbon dioxide (Air Liquide, $CO_2 \geq 99.995\%$) or labeled $^{13}CO_2$ (Sigma–Aldrich, 99% atom ^{13}C) previously saturated with water vapour at 40 °C.

The loaded vial was closed and left for 10 min at ambient temperature (23 °C) for adsorption/desorption equilibrium before irradiation using an XBO lamp for the planned time. The vial was then heated to 60 °C while closed and the gaseous products of the reaction were transferred to gas-chromatograph analyzers equipped with BID, TCD, or MS detectors. Details of the chromatographic determinations are given in the Supporting Information.

In the recycling test, the photocatalyst was collected, washed, dried and used again in a new cycle.

Results and Discussion

Wherever the designation "x%In_2O_3@g-C_3N_4" is used in the text, x% gives the percentage of In-metal loaded on g-C_3N_4 and not In_2O_3.

Structural and Morphological Characterization

Aerobic thermal treatment of melamine at 600 °C leads to the formation of graphitic carbon nitride, g-C_3N_4. When such treatment was carried out under aerobic heating in the presence of In(III)nitrate, In_2O_3@g-C_3N_4 was formed at different In_2O_3 loadings, depending on the amount of In(III)nitrate used. Figure 2 shows the XRD patterns of the so prepared pure g-C_3N_4 and 2%In_2O_3@g-C_3N_4.

The most intense peak at $2\theta = 27.5°$ is reported as the (002) plane of graphitic carbon nitride - due to stacking of layers of conjugated aromatic systems. The less intense peak at 12.7° is due to the layered packing structure of tri-s-triazine units and can be assigned to the (100) plane as previously reported[30] in JCPDS 87-1526 card. Additional X-ray diffraction peaks match with the JCPDS card no. 06-0416 - standard data file of indium oxide (In_2O_3), confirming the formation of the cubic bixbyite crystal structure of In_2O_3 with the Ia-3 space group. The XRD patterns of samples with different indium load show all the same two phases: graphitic carbon nitride and cubic bixbyte crystal structure of In_2O_3. The average crystallites sizes of both materials were determined using Scherrer's equation (Eq. 1) where D is the average crystallite size value, β is the full width at half maximum (FWHM) of the diffraction peak, λ is the wavelength of radiation, and θ is the Bragg's angle.

$$D = \frac{0.9\lambda}{\beta \cos\theta} \quad (1)$$

The average crystallite size of non-modified g-C_3N_4 was 10 nm, the size of g-C_3N_4 in In_2O_3@g-C_3N_4 composite was just slightly smaller (9.3 nm), and the size of In_2O_3 particles was 8.4 nm.

The surface microscopic morphology of In_2O_3@g-C_3N_4 was studied by SEM. Figure 3 shows that the graphitic carbon nitride material is stacked by irregularly layered nanosheets.

Particles of indium oxide are clearly visible on the surface of g-C_3N_4 as light spots and they are aggregated into relatively large structures (up to 100 nm). Figure S1 in Supporting Information shows SEM-EDS mapping of nitrogen, oxygen, indium, and carbon in 10%In_2O_3@g-C_3N_4 demonstrating the homogeneous distribution of the elements.

Spectroscopic Analysis

Both graphitic carbon nitride and indium-modified graphitic carbon nitride are yellowish materials. Diffuse reflectance UV-Vis spectra of the materials were measured to determine the optical absorption range. DRS spectra were transformed to the Kubelka-Munk function, shown in Figure 4A. g-C_3N_4 itself shows absorption starting at *ca.* 450 nm, as previously reported.[6,31] Band gap energies calculated from Tauc plots (Figure 4B) are given in Table 1.

The addition of In_2O_3 up to 2% In/g-C_3N_4 does not significantly change the spectrum. In particular, it does not significantly increase the light absorption range, as often observed in case of doped materials.[6] Such a trend can be explained considering that neat In_2O_3 is a material with an absorption range starting itself at *ca.* 450 nm (spectrum in

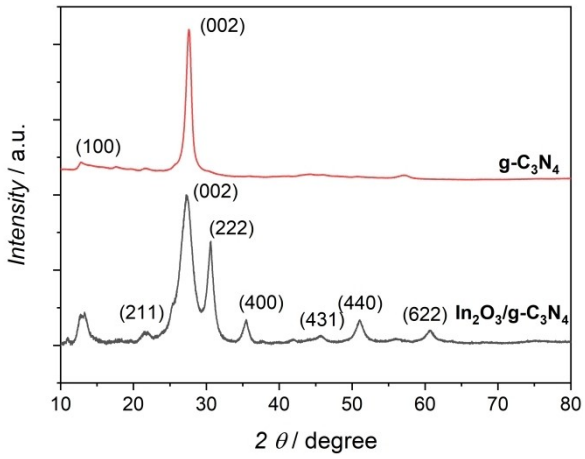

Figure 2. X-ray diffraction patterns of g-C_3N_4 (upper graph) and 2%In_2O_3@g-C_3N_4 (lower graph).

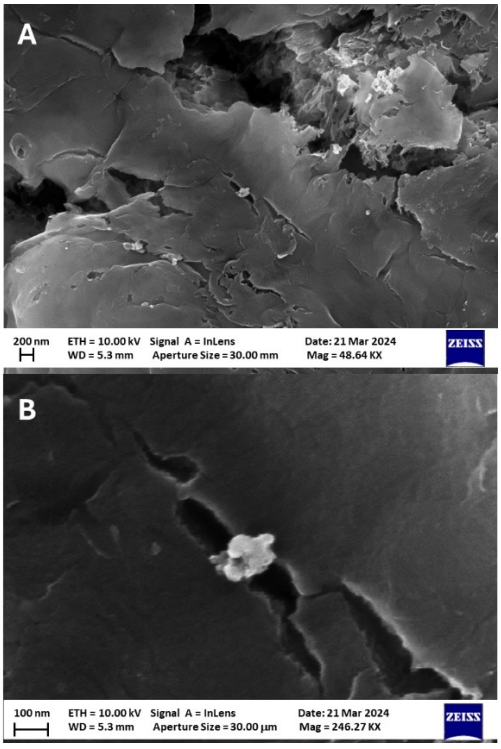

Figure 3. SEM analysis of 2%In_2O_3@g-C_3N_4. A) (200 nm) and B) (100 nm) show the same sample at different scale. White particles are In_2O_3 aggregates.

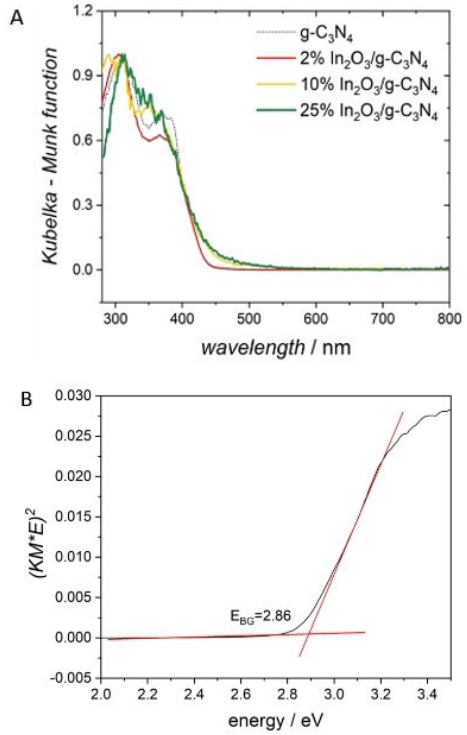

Figure 4. UV-Vis spectra of g-C_3N_4 and In_2O_3@g-C_3N_4. A) Kubelka-Munk function. B) Determination of band gap energy (E_{BG}) from Tauc plot for 2% In_2O_3@g-C_3N_4.

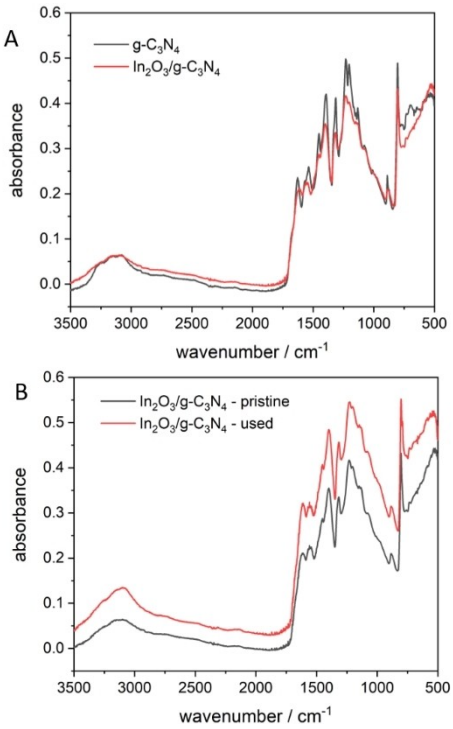

Figure 5. FTIR analysis. A) comparison between pristine g-C_3N_4 and 2% In_2O_3@g-C_3N_4. B) Comparison between 2%In_2O_3@g-C_3N_4 and the same sample after 1 h use in a photocatalytic reaction.

Table 1. Band gap energies of starting and composite materials.

Material	Band gap energy ± 0.05 eV
g-C_3N_4	2.90 eV
2%In_2O_3@g-C_3N_4	2.86 eV
10%In_2O_3@g-C_3N_4	2.60 eV
25%In_2O_3@g-C_3N_4	2.54 eV
In_2O_3	2.79 eV

Figure S2) – covering the absorbance range of g-C_3N_4. However, higher amount of indium oxide on g-C_3N_4 leads to a substantial decrease of the band gap energy, even below the value of indium oxide. This suggests the formation of new chromophore species.

FTIR spectra of unmodified and modified materials are shown in Figure 5 (g-C_3N_4 and 2%In_2O_3@g-C_3N_4) and Figure S3 (photocatalyst with 10% and 25% of In). The spectrum of neat g-C_3N_4 matches well with literature data.[6,32] The band in the range 800–1200 cm^{-1} corresponds to the stretching vibrations of the C–N bonds within the heptazine units of g-C_3N_4. The bands around 1200–1600 cm^{-1} are associated with the stretching vibrations of the C=C and C=N bonds. These vibrations are indicative of the aromatic system present in the g-C_3N_4 structure. Furthermore, the region between 3000–3500 cm^{-1} shows the peak related to the N–H stretching vibrations, which are usually due to amino groups or other N,H-containing functionalities present on the surface of g-C_3N_4. Modification of graphitic carbon nitride with In_2O_3 does not significantly change the FTIR spectrum. However, it is well visible that all bands are less sharp. Broadening of bands can suggest the interaction of g-C_3N_4 with In_2O_3, which spectrum is shown in Figure S4. Materials loaded with a high amount (10 and 25% In) of indium oxide show a weak band at about 2100–2200 cm^{-1} that could be attributed to the nitrile species,[33] originated from a ring opening process. The intensity of the band slightly increases with increasing the amount of In_2O_3 suggesting that the thermal condensation of melamine in the presence of large amounts of indium species somehow affects the structure of g-C_3N_4, even if at very limited extension. Noteworthy, the IR spectrum of the composite run after 1 h of use in photocatalysis shows that the material maintains its original structure (Figure 5B).

Electrochemical and Photoelectrochemical Properties

Electrochemical and photoelectrochemical properties of the In_2O_3@g-C_3N_4 material were studied using several techniques including cyclic voltammetry, OPC determination, chronoamperometric analysis under chopped light as well as electrochemical impedance spectroscopy. Figure S5 shows the open circuit potential (OCP) of the In_2O_3@g-C_3N_4 under dark and light conditions, revealing a photocathodic behavior, since the OCP increases (towards positive potentials) under illumination. This is not the typical behavior of graphitic carbon nitride, for which a decrease of OCP under light was reported.[34] Such change

must be ascribed to the presence of In_2O_3 in the doped material and the formation of the *n,n*-heterojunction.

Cyclic voltammetry (Figure S6) confirms a high electrochemical stability of the new material In_2O_3@g-C_3N_4 under anodic conditions and a lower stability under cathodic polarization. Such result is due to the reinforcing effect of the two *n*-type semiconductors. The results of photoelectrochemical chronoamperometric analysis, performed under chopped light (light pulse followed by dark time), are shown in Figure 6. In photoelectrochemical measurements, both, neat g-C_3N_4 and that modified with indium oxide, exhibit the unique ability to generate cathodic photocurrents when exposed to light. Cathodic photocurrents start from about +0.15 V *vs* Ag/AgCl. In general, the net density of photocurrents increases with decreasing the potential. Noteworthy, the density of photocurrent generated by In_2O_3@g-C_3N_4 (at 2% and 10% In-loading) is noticeably higher than that of non-modified g-C_3N_4. 25% In_2O_3@g-C_3N_4 exhibits a lower density of generated photocurrents, but they are stronger at more positive voltage.

The Mott-Schottky plot (Electrochemical Impedance Spectroscopy) is a technique used in electrochemistry to determine the flat band potential of a semiconductor-electrolyte interface. Flat band potential is the potential at which the semiconductor is in equilibrium with the electrolyte, and there is no net movement of charge carriers across the interface. The slope of the Mott-Schottky plot (Figure 7) is related to the doping concentration. A positive slope of plot is typical for *n*-type semiconductors.

The flat band potential was determined by the x-axis intercept of the plot. In the present case, the flat band potential was −1.11 V *vs* Ag/AgCl (−0.91 V *vs* Normal Hydrogen Electrode, NHE): it is comparable with literature data reported by L. Cao for pure g-C_3N_4 (equal to −1.01 V vs Ag/AgCl).[35] However, to the best of our knowledge Mott–Schottky analysis was never published for a In_2O_3@g-C_3N_4 composite. This is, thus, the first ever report for such *n,n*-junction.

Photocatalytic Activity Towards Gas-Phase CO_2 Reduction in Presence of Water-Vapor

Irradiation of CO_2 and water-vapor in the presence of In_2O_3@g-C_3N_4 leads to the formation of carbon monoxide, methane and methanol (tests in gas phase). Figure 8 shows a comparison of results obtained using modified and non-modified graphitic carbon nitride. Carbon monoxide was the major product of carbon dioxide reduction with all catalysts. Interestingly, In_2O_3@g-C_3N_4 increases the production of methanol and methane, in comparison with the pristine g-C_3N_4. In absence of CO_2, each photocatalyst showed activity towards the reduction

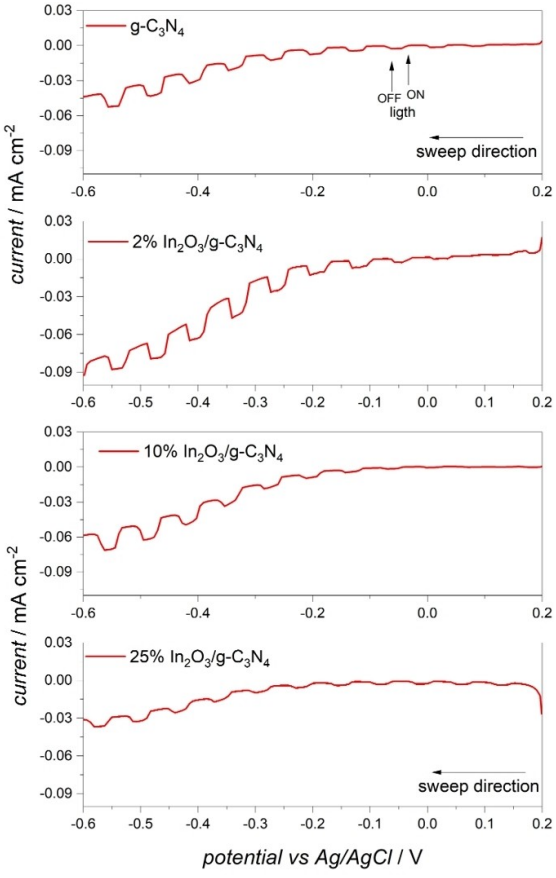

Figure 6. Photocurrent analysis: indium-modified and neat g-C_3N_4 performed in 0.1 M phosphate buffer (pH 7). Potential sweep: from anodic to cathodic. Light pulses are indicated by arrows.

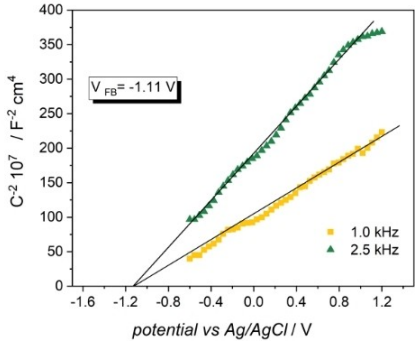

Figure 7. Mott–Schottky plots obtained for 2%In_2O_3/g-C_3N_4 at two different frequencies. Measurements were performed in electrolyte at pH 7, in dark. Sweep direction: from positive to negative potentials.

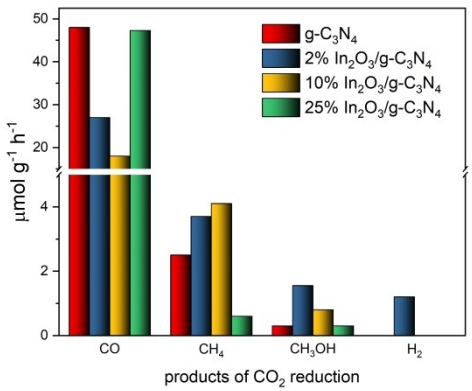

Figure 8. Results of photocatalytic tests performed using In_2O_3@g-C_3N_4 at different indium-loading on g-C_3N_4.

of water to hydrogen (14 $\mu mol\,g^{-1}\,h^{-1}$). The evolution of hydrogen was noticeably lower (less than 2 $\mu mol\,g^{-1}\,h^{-1}$) in presence of CO_2. The amount of reduced carbon dioxide was: 50.80 $\mu mol\,g^{-1}\,h^{-1}$ in case of g-C_3N_4; 32.25 $\mu mol\,g^{-1}\,h^{-1}$ in case of 2%In_2O_3@g-C_3N_4, 23.14 $\mu mol\,g^{-1}\,h^{-1}$ in case of 10%In_2O_3@g-C_3N_4, and 48.2 $\mu mol\,g^{-1}\,h^{-1}$ in case of 25%In_2O_3@g-C_3N_4. To the decrease of CO production with catalysts loaded at 2 and 10% In, corresponds an increase of production of hydrogenated forms, i.e. CH_3OH and CH_4. Such data suggest that the *n,n*-type junction improves the performance of the catalyst towards the "coupled electron plus proton transfer" to CO_2. Why at highest loading of In_2O_3 (25% In) the material exhibited lower efficiency in methane and methanol production in comparison with 2% and 10% indium, and a CO production close to that of neat g-C_3N_4 deserves further structural and catalytic investigations.

Two types of stability tests were performed: a) long term irradiation and b) recycling tests (Figure 9). A stability test for the photocatalytic activity of In_2O_3/g-C_3N_4 in CO_2RR was conducted, revealing good performance over 6 h (Figure 9A). The catalyst even maintained its efficiency in a recycling test, (Figure 9B) demonstrating consistent CO_2 conversion rates and stable production of reduction products. The stability of In_2O_3/g-C_3N_4 was demonstrated by its structural integrity and due to the strong interaction between In_2O_3 and g-C_3N_4, which prevents significant degradation or deactivation of the active sites. This sustained activity underscores the potential of In_2O_3/g-C_3N_4 as a durable and effective photocatalyst for long-term applications in CO_2 reduction processes.

As discussed above, the FTIR spectrum of the material 2% In_2O_3@g-C_3N_4 recovered after the photocatalytic test in gas-phase (Figure 5B) does not show any difference with respect to the freshly prepared material, confirming its stability under the operative conditions and its potential recyclability.

Graphitic carbon nitride contains carbon atoms that, under irradiation, can be extracted from the structure and transformed into various C_1 compounds, potentially leading to false conclusions regarding CO_2 reduction. Experiments with labelled carbon dioxide ($^{13}CO_2$) have been performed to confirm that the observed C_1 compounds are products of photocatalytic CO_2 reduction. The GC-MS of the reaction gas mixture shows that the peak at 1.19 min can be assigned to methanol (which partially overlaps the CO and CO_2 peaks that are not well separated in GC-MS while they are using BID), by comparison with an authentic sample. The MS spectrum taken for this peak is shown in Figure 10.

However, all peaks of $^{13}CH_3OH$ are observed: 34, 33, 32, 31, 30, plus the peak at 29 m/z due to ^{13}CO. Among them, peaks at m/z 33 and 31 are fingerprints of the PCET (Proton Coupled to

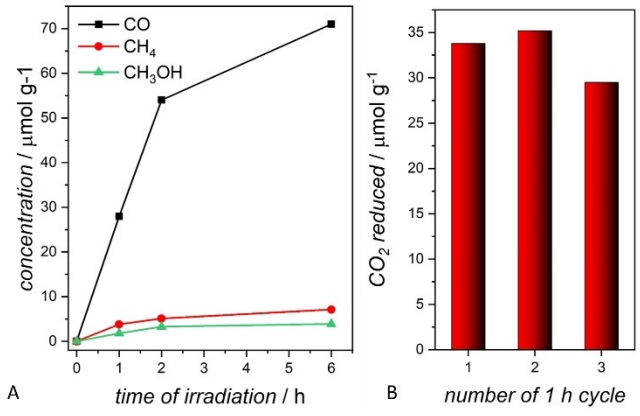

Figure 9. Stability tests performed using 2%In_2O_3@g-C_3N_4 catalysis. A) Evolution of CO_2 reduction products during 6 hour tests. B) Summarized amount of reduced CO_2 during a 1 hour test using a recycled photocatalyst.

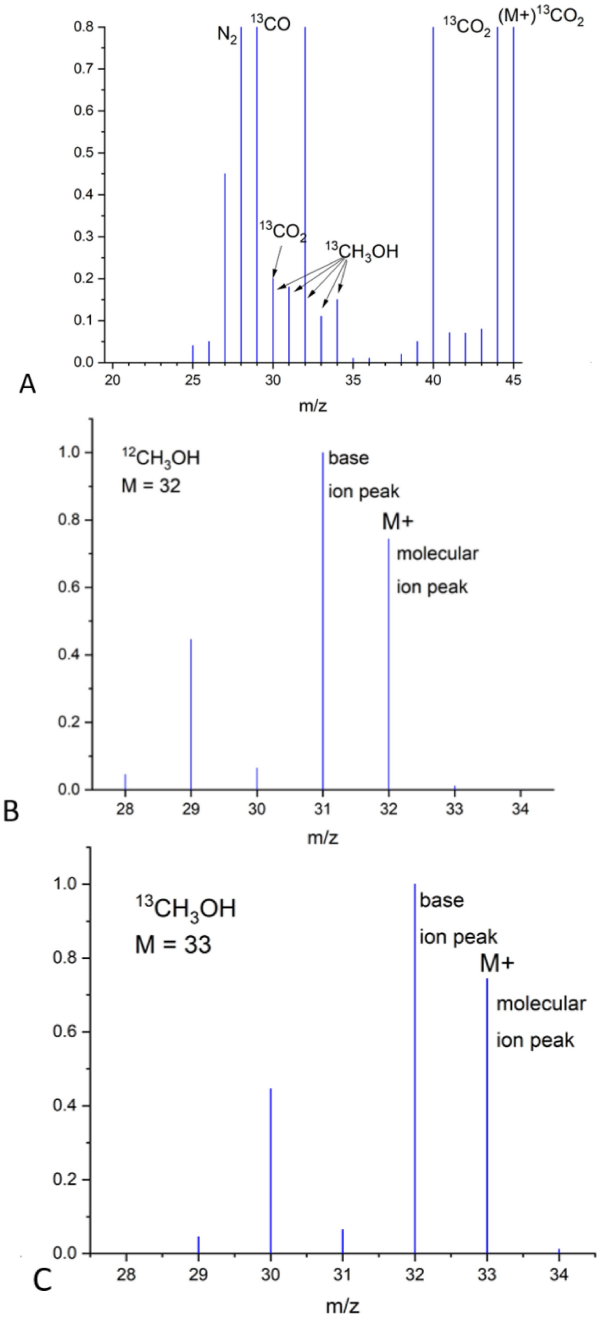

Figure 10. MS fragmentation spectrum of $^{13}CH_3OH$ obtained in the photocatalytic test under 2%In_2O_3@g-C_3N_4 catalysis (A) compared with that of $^{12}CH_3OH$ (from Shimadzu LabSolution database) (B) and $^{13}CH_3OH$ (from Shimadzu database) (C). The peak at 40 m/z in A is due to a standard used in GC.

Electron Transfer) reduction of $^{13}CO_2$ as they do not exist in any other possible labeled or not-labeled products. Therefore, the MS-spectrum confirms the formation of methanol from labelled ^{13}C-carbon dioxide, excluding any interference of the catalytic material.

Discussion

The low photoactivity of a single photocatalyst is often associated with decay processes such as relaxation and electron-hole recombination.[36] The construction of hetero junction-photocatalysts is aimed at charge separation stabilization and promoting the electron and proton transfer to the substrate to be reduced.[37,38] Type II heterojunctions, Z-scheme heterojunctions, and S-scheme heterojunctions are the most commonly known.[39] Usually, *p,n*-junctions are built in order to promote both reduction processes of the substrate and (water) oxidation.

The thermal condensation of melamine in presence of metal salts [for example iron(III)nitrate, bismuth(III)nitrate, manganese-(II)nitrate, cobalt(II)nitrate, zinc nitrate or antimony(III) sulfate] results in the formation of graphitic carbon nitride doped with metal ions.[6,22] Previously described photocatalytic materials exhibit a single phase with extended range visible light absorption. Here we have found that the thermal transformation of melamine in the presence of indium nitrate leds to the formation of the two-phase composite photocatalyst – In_2O_3@g-C_3N_4 – formed by two *n*-type semiconductors. The structure of the so-obtained *n,n*-composite has been determined by XRD analysis. The 2%In_2O_3@g-C_3N_4 composite shows absorption of light within the visible light range and a band gap equal to 2.86 eV, that corresponds to light absorption onset at 433 nm. Interestingly, the conduction band-potential of g-C_3N_4 is more negative than that of In_2O_3. Therefore, at the *n,n*-heterojunction of the two semiconductors, electrons keep on flowing from electron-rich graphitic carbon nitride to indium oxide until the Fermi levels of the two components become coincident (Figure 11). With increasing the amount of indium oxide, we have observed a progressive decrease of the band gap energy down to 2.54 eV (25% In-loading on g-C_3N_4), that is lower that E_{BG} of In_2O_3. This band gap energy can be attributed to the direct transition of electrons from the valence band of g-C_3N_4 to conduction band of In_2O_3 (see central arrow in Figure 10). An opposite direct Z-scheme was proposed recently for a TiO_2@g-C_3N_4 composite (flow of excited electrons from CB of TiO_2 to VB of g-C_3N_4).[40]

In this way, an accumulation of negative charges is generated onto In_2O_3, that can play the role of active center for photocatalytic reduction reactions such as CO_2 reduction or water reduction. Such hypothesis is also supported by the observed higher density of photocurrents of the composite with respect to g-C_3N_4 alone. Such negative charge can also enhance the binding of CO_2 to In through the C-atom, making it prompt to protonation and reduction to CO.

The literature reports a few examples of *n,n*-heterojunction of two semiconductors, but none includes g-C_3N_4. They can behave as type II, Z-scheme or S-scheme heterojunctions. Examples are: InP/GaAs,[41] TiO_2/Fe-MOF,[42] $Ag_3PO_4/Co_3(PO_4)_2$,[43] $In_2S_3/BiVO_4$,[44] or the most common TiO_2/ZnO.[45] Noteworthy, no one of them was used in gas-phase CO_2-H_2O co processing to afford energy products from CO_2. The determined effective conduction band potential of the new composite is equal to −0.91 V *vs* NHE: the so formed electrons have enough energy to perform multielectron reduction of CO_2. The potential of selected reactions is reported in Table 2.[46]

The experimental results show that carbon dioxide is photocatalytically reduced in the gas phase in presence of water vapor to afford carbon monoxide (Eq. (2), major product) and other C_1 compounds (CH_3OH and CH_4). On the other hand, the potential of photogenerated hole is sufficient for water oxidation. According to our best knowledge this is the first example of photocatalytic reduction of CO_2 using water as the only electron source promoted by a In_2O_3@g-C_3N_4 composite. The reduction of CO_2 to CO and of water to hydrogen require both 2-electrons and imply two protons, while the reduction of CO_2 to CH_3OH or CH_4 requires six- and eight-electrons, respectively, coupled to proton-transfer (6 and 8, respectively). Comparing pure g-C_3N_4 and the In_2O_3@g-C_3N_4 composite, it comes out that the latter is a better promoter of both the multielectron-transfer and PCET, favoring the formation of hydrogenated species such as CH_3OH and CH_4 with respect to CO (Figure 8). This is an interesting finding as methanol and methane have higher value than CO, laying on the border of the chemical-energy sectors. Noteworthy, the multi-electron-proton transfers to afford methanol or methane, that imply a lower energy (see Table 2) with respect to the reduction to CO, can be opposed by kinetic factors bound to the sequential electron-proton transfer that may prevent the formation of

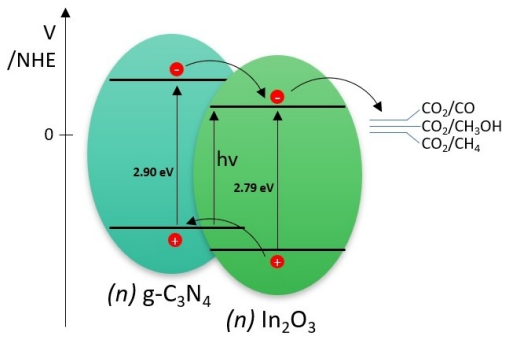

Figure 11. Expected mechanism of In_2O_3@g-C_3N_4 photocatalytic reduction of CO_2.

Table 2. Reduction potential of CO_2 to various C_1 products.

$CO_2+2H^++2e^-\rightarrow HCOOH$	$E^0=-0.61$ V	(1)
$CO_2+2H^++2e^-\rightarrow CO+H_2O$	$E^0=-0.52$ V	(2)
$CO_2+4H^++4e^-\rightarrow HCHO+H_2O$	$E^0=-0.48$ V	(3)
$CO_2+6H^++6e^-\rightarrow CH_3OH+H_2O$	$E^0=-0.38$ V	(4)
$CO_2+8H^++8e^-\rightarrow CH_4+H_2O$	$E^0=-0.24$ V	(5)

hydrogenated species and by the stability of the photocatalyst-CO bond.

Comparing the amount of reduced carbon dioxide shown in Figure 9 with the calculated numbers of electrons transferred from excited photocatalysts to CO_2 to produce CO, CH_4 and CH_3OH (calculations given in Table S1) one can infer that:

- the non-modified graphitic carbon nitride produces approximately 17% higher transfer of electrons to CO_2 that results essentially in the formation of CO;
- indium oxide promotes the multielectron-transfer and PCET, that results in a more than five-fold increase of methanol formation by the composite with respect to neat g-C_3N_4;
- the loading of In is critical and increasing the amount of In@g-C_3N_4 does not increase the PCET.

This latter aspect is under study in order to rationalize the behaviour of the composite and improve its photocatalytic activity and selectivity towards a target product.

The electron-rich g-C_3N_4 mainly promotes the formation of CO (a "$2e^- + 2H^+$" process), which implies the binding of CO_2 to the photomaterial through the C-atom (g-$C_3N{\rightarrow}CO_2$), which acts as electron-density acceptor. Protonation at either oxygen atom of the bound-CO_2 followed by e-transfer ("$H^+ + e^-$") promotes the formation of CO and water (Scheme 1).[47] Formed CO is easily released from the catalyst surface.

The addition of In_2O_3 modifies the overall potential of the material and even the mechanism can be modified towards the formation of In-OCH_3 bond which affords methanol (a "$6H^+ + 6e^-$" process) and, possibly, methane (an "$8H^+ + 8e^-$" process). For promoting the multielectron process, the reducing moiety must be more tightly bound to the catalyst and the In-OR bond intervenes. The reduction potential of CO_2 to CO (−0.53 V), CH_3OH (−0.38 V) and CH_4 (−0.24 V) are anyway quite close (Table 2) and, therefore, such processes can be quite concomitant. Anyway, we emphasize here that the various reduction processes are preferentially promoted by different actors.

Noteworthy, carbon dioxide is the source of the reduced products and not the carbon derived from a possible decomposition of the photocatalyst or from serendipitous contaminants, as demonstrated by the use of $^{13}CO_2$ that has allowed to identify labeled $^{13}CH_3OH$ (and ^{13}CO) as the only methanol (and CO) form present in the reaction mixture excluding, thus, any other possible source of carbon than $^{13}CO_2$.

The new material is stable and can be recovered unaltered and reused in consecutive photocatalytic runs. Its performance needs deeper understanding with respect to most performing composition that must be engineered accordingly. Nevertheless, the new *n,n*-junction composite shows enough new properties with respect to the pristine g-C_3N_4 and other similar composites, mainly the stability and the promotion of multi-electron-multi proton transfer to CO_2 and its reduction in the absence of sacrificial e-donors. As a final note, we recall that

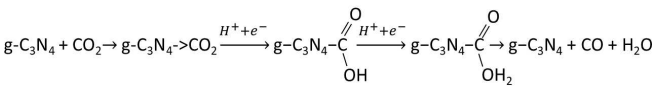

Scheme 1. Double "$H^+ + e^-$" transfer to CO_2 to generate CO.

In_2O_3 under photothermal conditions (250–300 °C under white light) promotes the Reverse Water Gas Shift Reaction (1:1 CO_2-H_2 mixture)[44] with a conversion of $<20\ \mu mol\ g^{-1}\ h^{-1}$, that is much increased when defective black In_2O_3 is used. In our process, water is used as source of electrons and protons at ambient temperature.

Acknowledgements

This work was financed by EU within the Horizon Europe Research Programme – DESIRED project (project code: 101083355). Progetto Competitivo MIUR CMPT212338 is also gratefully acknowledged. The authors thank Mr. Domenico Caringella for some experimental assistance during his Bachelor Thesis in Material Sciences at Uniba.

Conflict of Interests

The authors declare no conflict of interest.

Data Availability Statement

The data that support the findings of this study are available from the corresponding author upon reasonable request.

Keywords: carbon dioxide reduction · coprocessing of CO_2 – H_2O · indium(III) oxide · graphitic carbon nitride · *n,n*-junctions

[1] E. Wierzyńska, K. Korytkowska, K. Kazimierczuk, T. Łęcki, K. Zarębska, K. P. Korona, M. Pisarek, B. Furtak, M. Skompska, *J. Phys. Chem. C* **2024**, *128*, 894–907.
[2] M. Bellardita, E. I. García-López, G. Marcì, I. Krivtsov, J. R. García, L. Palmisano, *Appl. Catal. B* **2018**, *220*, 222–233.
[3] S. Wojtyła, K. Szmit, T. Baran, *J. Inorg. Organomet. Polym.* **2018**, *28*, 492–499.
[4] A. Dandia, S. L. Gupta, P. Saini, R. Sharma, S. Meena, V. Parewa, *Curr. Res. Green Sustain. Chem.* **2020**, *3*, 100039.
[5] G. Dong, Y. Zhang, Q. Pan, J. Qiu, *J. Photochem. Photobiol. C* **2014**, *20*, 33–50.
[6] S. Wojtyła, K. Śpiewak, T. Baran, *J. Photochem. Photobiol. A* **2020**, *391*, 112355.
[7] E. Fernandes, P. Mazierski, T. Klimczuk, A. Zaleska-Medynska, R. C. Martins, J. Gomes, *Catalysts* **2023**, *13*, 789.
[8] D. Pradhan, L. Mohanty, R. Singhal, E. Falletta, S. K. Dash, *Inorg. Chem. Commun.* **2023**, *156*, 111259.
[9] E. I. García-López, L. Palmisano, G. Marcì, *Chem. Eng.* **2023**, *7*, 11.
[10] M. T. A. Iapichino, R. Fiorenza, V. Patamia, G. Floresta, A. Gulino, M. Condorelli, G. Impellizzeri, G. Compagnini, S. Sciré, *Catal. Commun.* **2024**, *187*, 10.1016/j.catcom.2024.106850.
[11] E. I. García-López, A. Genco, V. Lagostina, M. C. Paganini, G. Marcì, *Catal. Today* **2023**, *423*, 114283.
[12] S. Wojtyła, T. Baran, *Nano Select* **2021**, *2*, 389–397.
[13] L. Peng, H. Wang, G. Li, W. Zhang, Z. Liang, T. An, *Appl. Catal. B* **2023**, *329*, 122580.
[14] M. R. Miroliaei, A. Dadfarma, M. Shahabi-Nejad, E. Jalali, H. Sheibani, *Braz. J. Chem. Eng.* **2023**, 10.1007/s43153-023-00374-3.
[15] N. Sangiorgi, G. Tuci, A. Sanson, M. Peruzzini, G. Giambastiani, *Rend. Fis. Acc. Lincei* **2019**, *30*, 497–513.
[16] K. R. Reddy, C. H. V. Reddy, M. N. Nadagouda, N. P. Shetti, S. Jaesool, T. M. Aminabhavi, *J. Environ. Manage.* **2019**, *238*, 25–40.
[17] M. Aresta, A. Dibenedetto, *J. CO2 Util.* **2024**, *80*, 102688.

[18] M. Aresta, *Greenhouse Gases: Science and Technology* **2019**, *9*, 610–612.
[19] E. Gong, S. Ali, C. B. Hiragond, H. S. Kim, N. S. Powar, D. Kim, H. Kim, S.-I. In, *Energy Environ. Sci.* **2022**, *15*, 880–937.
[20] W. Wan, Q. Zhang, Y. Wei, Y. Cao, J. Hou, C. Liu, L. Hong, H. Gao, J. Chen, H. Jing, *Chem. Eng. J.* **2023**, *454*, 140122.
[21] M. Bellardita, V. Loddo, F. Parrino, L. Palmisano, *ChemPhotoChem* **2021**, *5*, 767–791.
[22] S. Wojtyła, K. Śpiewak, T. Baran, *J. Inorg. Organomet. Polym.* **2020**, *30*, 3418–3428.
[23] X. Yang, W. Yu, W. Wang, D. Wang, Q. Wang, X. Huo, *Int. J. Hydrogen Energy* **2023**, *48*, 35599–35609.
[24] D. Sariket, A. Maity, S. Kundu, C. Bhattacharya, *J. Solid State Chem.* **2022**, *315*, 123484.
[25] W. Liu, J. Zhang, Q. Kang, H. Chen, R. Feng, *Ecotoxicol. Environ. Saf.* **2023**, *252*, 114611.
[26] Y. Zhao, Y. Song, S. Sun, S. Yao, L. Wang, W. Li, S. Li, *J. Water Proc. Eng.* **2024**, *59*, 105021.
[27] X. Chen, Y. Jin, P. Huang, Z. Zheng, L.-P. Li, C.-Y. Lin, X. Chen, R. Ding, J. Liu, R. Chen, *Appl. Catal. B* **2024**, *340*, 123235.
[28] L. Wang, Y. Chen, C. Zhang, Z. Zhong, L. Amirav, *ACS Appl. Mater. Interfaces* **2024**, *16*, 4581–4591.
[29] D. M. S. Marcolongo, F. Nocito, N. Ditaranto, R. Comparelli, M. Aresta, A. Dibenedetto, *Catalysts* **2022**, *12*, 153.
[30] X. Bai, L. Wang, R. Zong, Y. Zhu, *J. Phys. Chem. C* **2013**, *117*, 9952–9961.
[31] E. Wierzyńska, M. Pisarek, T. Łęcki, M. Skompska, *Molecules* **2023**, *28*, 2469.
[32] S. Pareek, M. Sharma, S. Lal, J. K. Quamara, *J. Mater. Sci. Mater. Electron.* **2018**, *29*, 13043–13051.
[33] X. She, J. Wu, J. Zhong, H. Xu, Y. Yang, R. Vajtai, J. Lou, Y. Liu, D. Du, H. Li, P. M. Ajayan, *Nano Energy* **2016**, *27*, 138–146.
[34] J. Rusek, Š. Paušová, P. Praus, J. Krýsa, *Catalysts* **2021**, *11*, 203.
[35] L. Cao, Y. Li, Z. Zheng, *J. Mater. Sci. Mater. Electron.* **2022**, *33*, 479–489.
[36] V. Etacheri, C. Di Valentin, J. Schneider, D. Bahnemann, S. C. Pillai, *J. Photochem. Photobiol. C* **2015**, *25*, 1–29.
[37] L. Schumacher, R. Marschall, *Top. Curr. Chem. (Z)* **2022**, *380*, 53.
[38] K. Afroz, M. Moniruddin, N. Bakranov, S. Kudaibergenov, N. Nuraje, *J. Mater. Chem. A* **2018**, *6*, 21696–21718.
[39] W. Fang, L. Wang, *Catalysts* **2023**, *13*, 1325.
[40] J. Liu, B. Cheng, J. Yu, *Phys. Chem. Chem. Phys.* **2016**, *18*, 31175–31183.
[41] W. G. Oldham, A. G. Milnes, *Solid-State Electron.* **1963**, *6*, 121–132.
[42] S. Feizpoor, A. Habibi-Yangjeh, R. Luque, *Chemosphere* **2023**, *336*, 139101.
[43] R. Bagtache, A. M. Djaballah, K. Lachekhab, Y. Bouchefa, M. Trari, *Chem. Phys. Lett.* **2024**, *839*, 141112.
[44] B. Baral, S. Mansingh, K. H. Reddy, R. Bariki, K. Parida, *ACS Omega* **2020**, *5*, 5270.
[45] A. Kubiak, S. Żółtowska, A. Bartkowiak, E. Gabała, N. Sacharczuk, M. Zalas, K. Siwińska-Ciesielczyk, T. Jesionowski, *Materials* **2021**, *14*, 6063.
[46] E. Fujita, *Coord. Chem. Rev.* **1999**, *185–186*, 373–384.
[47] M. Aresta, E. Quaranta, I. Tommasi, *J. Chem. Soc. Chem. Commun.* **1988**, 450–452.

Manuscript received: March 27, 2024
Revised manuscript received: May 21, 2024
Accepted manuscript online: May 24, 2024
Version of record online: ■■, ■■

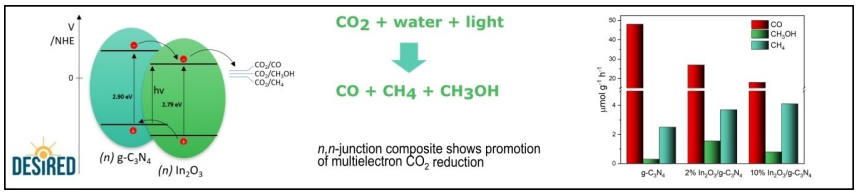

The article presents In_2O_3@g-C_3N_4 composite photocatalyst synthesis. Its n,n-heterojunction enhances charge separation, facilitating CO_2 reduction to CH_4, and CH_3OH. While efficiency matches neat g-C_3N_4, potential exists for further optimization, confirmed by labeled $^{13}CO_2$ exclusion of photocatalyst decomposition or contaminant degradation.

T. Baran, M. Aresta, R. Comparelli, A. Dibenedetto**